Mechanical properties of submicronic and nanometric boron carbides obtained by Spark Plasma Sintering influence of B/C ratio and oxygen content

L. Roumiguier, A. Jankowiak, N. Pradeilles, G. Antou, A. Maître

Version of Record: https://www.sciencedirect.com/science/article/pii/S0272884219303220
Manuscript_08e4207dc7bd5dbabf2d99d502dbd517

Mechanical properties of submicronic and nanometric boron carbides obtained by Spark Plasma Sintering: influence of B/C ratio and oxygen content

L. Roumiguier [a,b], N. Pradeilles [b], G. Antou [b], A. Jankowiak [a], A. Maître [b]

[a] DEN-Service de Recherches Métallurgiques Appliquées, CEA, Université Paris-Saclay, F-91191, Gif-sur-Yvette, France.

[b] Univ. Limoges, CNRS, IRCER, UMR 7315, F-87000 Limoges, France.

Corresponding author: Léna Roumiguier

- E-mail address: lena.roumiguier@unilim.fr
- Postal address: CEA Saclay, DEN/DANS/DMN/SRMA/LTMEx, Bâtiment 460 – PC 52, 91191 Gif-sur-Yvette, France.
- Telephone number: (+33)169083560
- Fax number: (+33)169088252

Abstract

Boron carbide samples exhibiting nanometric and submicronic microstructure were sintered by Spark Plasma Sintering to investigate the effect of grain size on mechanical properties. The mechanical properties of sintered monoliths were characterized at the grain and macroscopic scales. Although nanostructured material exhibits finer grains than the submicronic material (*i.e.* mean diameter of 82 *vs.* 474 nm), its apparent rigidity and hardness are found to be reduced by 6.8 % and 8.4 % respectively. This contradiction with the Hall-Petch law is linked to the chemical compositions of both materials, which show significant difference in terms of B/C ratio and higher structural oxygen content especially for nanostructured material.

Key words: Boron carbide; Mechanical properties (C), Hardness (C), Carbides (D).

1. Introduction

Boron carbide presents high melting point (∽ 2500 °C), low density (2.52 g/cm^3), high hardness (30 GPa), high mechanical strength (∽ 350 MPa) and high neutron absorption cross section [1–3]. This combination of properties is of high interest for industrial applications, such as armoring systems [4], nuclear power plants [3], hard metal tools [5], automotive [6] or even for biomedical [7].

Currently, boron carbide is selected for its very high hardness in comparison with other ceramic materials. Fine grain size boron carbide materials are attractive from a mechanical point of view. Indeed, Hall-Petch effect is usually observed for metals and ceramics, according to which lowering the grain size leads to higher hardness and mechanical strength [8–11]. Consequently, achieving dense boron carbide ceramics with fine grain size could enhance mechanical properties. However, as a result of very strong covalent bonding, the manufacturing of fully dense boron carbide ceramic with limited grain growth remains challenging and requires dedicated sintering process. Indeed, even if the combination of high temperatures and long holding times has been applied to densify boron carbide by pressureless sintering, resulting materials still exhibit residual porosity [12,13]. Near fully dense relative boron carbide specimens have been sintered by hot pressing. However, grain coarsening due to long holding times was observed leading to mean grain size around 16.4 µm, while starting powder showed an initial average particle diameter of 2.9 µm [14].

Fully dense boron carbide ceramics with relative densities higher than 98 % associated with micrometric or submicrometric grain size distributions have been manufactured without sintering aids using Spark Plasma Sintering (SPS) [15–22].

Recently, Moshtaghioun *et al.* [23] have characterized hardness and fracture toughness of boron carbide samples sintered by SPS with different mean grain sizes in the range 0.12 to 17.2 µm. Fully dense materials were not achieved for finer grain sizes, but a correcting factor was used to take into account the residual porosity for the comparison of mechanical properties. Hardness was found to follow the Hall-Petch law in this range of grain size. Moreover, no evolution in terms of fracture toughness was observed mainly due to the transgranular fracture mechanism. This latter result was also described by Sairam *et al.* [17].

The purpose of this work was to compare the mechanical properties of same relative density sintered materials exhibiting either nanometric or submicronic mean grain size. The sintered samples were carefully characterized by coupling XRD, Raman, TEM and elemental chemical analyses. These characteristics were correlated with mechanical properties, *i.e.* elastic properties and hardness characterized at the grain and macroscopic scales.

2. Experimental procedures

Starting materials were two commercially powders exhibiting submicrometric (grade HD 20, H. C. Starck GmbH, Germany) and nanometric grains (Tekna Advanced Materials Inc., Canada), and named in the following HD and TK, respectively. The grain size distribution was determined using two different techniques according to the expected particle size scale. Laser diffraction particle size analyzer (Horiba-LA-950V2, Japan) was used for HD powder, while TK powder was analyzed by dynamic light scattering (Zetasizer Nano ZS, Malvern Instruments, UK). Specific surface areas were obtained using a volumetric adsorption analyzer (ASAP 2020 V4.00, Micromeritics

Instrument Corp., U.S.A.). Structural and morphological characterizations were conducted by Transmission Electron Microscopy (JEM-2100F, JEOL, Japan). Chemical composition was determined by elemental chemical analyses (EMIA-321V for carbon, and EMGA-830 for oxygen and hydrogen from HORIBA, Ltd., Japan). X-ray diffraction (XRD) analyses were conducted using a Bruker D8 Advance device (Germany; LYNXEYE XE-T detector, Cu-Kα radiation, Ni filter). The XRD pattern acquisition conditions are: angular step of 0.02°, time per step of 0.3 s, angle range 10–120°. Finally, Raman spectroscopy analyses (Renishaw Invia Reflex, UK) were conducted to obtain useful information related to chemical bonding and phase distribution in boron carbide compounds. Raman spectra were recorded from 100 to 1800 cm^{-1} using a wavelength of 532 nm.

Boron carbide powders were previously pressed into a 20 mm diameter graphite die under a uniaxial pressure of 30 MPa. Resulting green densities were 43 ± 2 % and 45 ± 1 % for TK and HD powders, respectively. Then, samples were sintered using a Dr. Sinter 825 SPS device (from Fuji Electronics Industrial Co. Ltd., Japan). To elaborate samples with various relative densities, sintering temperatures were selected in the range 1300-1650°C, with a dwell time of 5 minutes and a uniaxial pressure of 75 MPa. A heating rate of 200 $°C.min^{-1}$ was applied since it was usually reported that boron carbides sintered with heating rates below 100 $°C.min^{-1}$ were subjected to abnormal grain growth [18,19].

Density of sintered samples was determined by Archimedes' method in ethanol. Similar chemical analyses than the ones conducted on powders were carried out. Phases in presence were also determined by XRD and the local order by Raman

analyses. Sintered samples were cut axially, and the cross-section was polished up to 1 µm to characterize their microstructure. After being thermally etched, microstructure was observed by Scanning Electron Microscopy (FEG-SEM Quanta 450, FEI, Thermo Fisher Scientific, USA). Grain size distribution was determined by measuring the Feret's diameter on at least 200 grains.

Mechanical properties were characterized at the grain and macroscopic scales. Nano-indentation measurements were performed by using a XP diamond nanoindenter (Nano Indenter XP™, MTS Nano Instruments, USA) equipped with a Berkovitch tip. The applied load ranged from 0.5 to 1000 mN. At least 30 indentations were performed for each sample and results were averaged. The intrinsic Young's modulus and hardness were estimated using Oliver and Pharr's analysis technique [24]. Apparent hardness was measured using a Knoop indenter under a load of 300 g, and results were averaged from at least 10 indentations. Apparent elastic constants (*i.e.* Young's modulus, shear modulus and Poisson's ratio) were determined by ultrasonic pulse echography using 10 MHz transducers in transmission mode (WC37-10 and SW37-10, Ultran, State College, USA).

3. Results and discussion

3.1. Characterizations of raw powders

First of all, raw materials were carefully characterized. Boron carbide and boric acid phases have been identified in both powders by XRD analyses, as shown in **Figure 1**. Free carbon crystallized under the graphite structure is also clearly observed in the HD powder, but not in the TK one. Crystallinity level of the TK powder is also considered too low in order to be detected by XRD technique. In fact, the slight bumps located

between the boron carbide peaks around 20-25° and 36° are representative of a partially crystallized powder.

Figure 2 shows Raman spectra of starting powders. The spectra have been normalized from the boron carbide highest intensity band, which is located at 1090 cm^{-1}. The HD powder spectrum can be divided in three characteristic zones [25,26]: (i) two main peaks at 480 cm^{-1} and 532 cm^{-1}, which corresponds to the rotation of the chains and the libration of the icosahedra; (ii) a group of peaks from 650 to 900 cm^{-1} associated to intra-icosahedron vibrations; (iii) high frequency peaks (975, 1002 and 1030 cm^{-1}) related to chain stretching, chain-icosahedron and inter-icosahedron vibrations. Regarding TK powder spectrum, the low level of crystallinity leads to band broadening and very low intensity bands [27,28]. In addition, 1355 and 1575 cm^{-1} bands corresponding to carbon can be observed in both Raman spectra powders [29]. Their high intensity masks the other peaks, which can be distinguished with the zoom in **Figure 2**.

Figure 3 presents particle size distributions of studied powders. These distributions are provided as a function of number of particles. Typical SEM and TEM micrographs of powders are displayed in **Figure 4**. The TK powder exhibits a monodisperse grain size distribution centered on 150 nm. However, SEM observations reveal elementary spherical shaped particles with diameters around 20-50 nm, displayed in **Figure 4**.**b**, and confirmed the presence of agglomerates around 150 nm. This is confirmed by the XRD peaks analysis, as the application of the Scherrer relation leads to a crystallite size around 25 nm. Moreover, two types of particles have been observed as indicated in **Figure 4.f**: amorphous spherical particles labelled A and some hexagonal crystallized

particles labelled B. The presence of these amorphous particles is in accordance with the diffuse halo observed in the diffraction pattern of the TK powder, plotted in **Figure 4.d**, which confirms the partial amorphous state of the material. The grain size distribution of HD powder is represented in **Figure 3** and is centered on 300 nm, but some larger elementary particles are also present up to 1100 nm. In addition, as it can be observed in **Figure 4.a,** some fine elementary particles of 60 nm diameter can be observed by SEM. Therefore, the HD powder is mainly composed of elementary particles with size ranged from 200 to 600 nm and exhibits a few coarser particles around 1 µm.

Chemical analyses have been carried out for both powders and are depicted in **Table 1**. The amounts of oxygen, carbon and hydrogen have been directly measured, while boron content was deduced by subtraction. Significant amounts of hydrogen are detected in both powders: 0.19 wt% for HD and 0.35 wt% for TK. These results confirm the presence of the crystallized boric acid detected by XRD, as indicated in **Figure 1**. Moreover, a nanometric liquid is observed on particle surface of both powder particles, mentioned with black arrows in **Figure 4.f**. This layer could be attributed to the existence of native oxide or hydroxide phases. In the literature, it is commonly admitted that boron carbide particles exhibit oxide phases at their surfaces [12,13,30–32], but hydrogen content was not controlled and XRD analysis does not allow to distinguish boron oxide and boric acid. In this work, as hydrogen was detected in both powders, this surface layer is likely to be composed of boric acid. However, some boron oxide may be also a part of this amorphous layer. Besides, higher levels of oxygen and hydrogen were noticed in the TK powder in comparison to the HD one. This observation can be explained by its higher specific surface area (56 and 26 $m^2.g^{-1}$

for the TK and HD powders respectively), which generate higher chemical reactivity for surface oxidation and hydroxylation. Also, the carbon content ranges from 17.6 to 22.8 % depending on the powder.

3.2. Spark Plasma sintering ability of the raw materials

Finer XRD peaks and Raman bands are observed after sintering, especially for the TK powder, as displayed in **Figure 1** and **Figure 2** respectively. This refinement allows distinguishing a greater number of Raman bands related to boron carbide. It is assumed that further crystallization occurred in TK samples during sintering as suggested by these refinements and the disappearance of the slight bumps initially detected between the boron carbide XRD peaks for the TK powder. In addition, for both powders, there is no shift of XRD peaks after sintering, which suggests that the stoichiometry of the carbide phase did not vary significantly during SPS treatment. Despite boric acid is almost totally removed during sintering, some residual traces remain in the TK samples, as noted in **Figure 1**. This is attributed to partial surface oxidization due to the small grain size distribution in the case of the TK specimens. Besides, according to **Table 1**, both sintered samples contain some residual oxygen content. As boric acid volatilized, the most part of this remaining oxygen is considered to be structural and corresponds to a boron oxycarbide phase B_xCO_y in both samples. The calculated stoichiometries of the oxycarbide phases from elemental chemical analyses of sintered samples are $B_{3.83}CO_{0.04}$ for HD and $B_{4.59}CO_{0.18}$ for TK.

Besides, an increase of the Raman band intensities located between 750 and 900 cm^{-1} in **Figure 2** is observed as the B/C ratio increases. This effect has already been observed in the literature [33–35] for different boron-rich phases. However, this phenomenon has not been discussed and the amount of oxygen possibly present in

their boron carbide structures not studied. Raman bands above 600 cm^{-1} are associated to icosahedral modes of boron carbide and a substitutional disorder within the icosahedron could involve a broadening of those bands [33]. In addition, the broad low frequency band, peaked at around 250 and 320 cm^{-1}, is usually observed for bulk ceramics and can be attributed to an atomic configuration disorder like twin defects [36]. In fact, twins are commonly observed for boron carbide powders, located at the grain boundaries [37].

Figure 5 presents the evolutions of the normalized shrinkage rates during the SPS treatment of both powders. To obtain these curves, the displacements of the plunger were recorded during the sintering of powder compacts, at 1650 °C for the HD powder and at 1550 °C for the TK powder. To remove the thermal expansion contribution of graphite tools on the monitored displacement, the measured displacements have been corrected by subtracting the ones measured on dense boron carbide samples in the same SPS conditions. Then, the deduced shrinkage rates have been normalized by the heights of the powder beds. In the case of the TK powder, the presence of a higher amount of oxide liquid or gaseous phases at the surfaces of boron carbide particles coupled with finer particles seem to initiate the sintering at a lower temperature than the one encountered for the HD powder, as evidenced in **Figure 5**. In addition, Tekna powder exhibits slower shrinkage rates, displayed in **Figure 5**. The presence of surface oxides seems to prevent from sintering, in spite of the presence of finer particles. Moreover, for a same sintering temperature, TK is denser than HD, see **Table 2**.

The highest density achieved for the TK sintered sample was 2.40 $g.cm^{-3}$ at 1550 °C, while higher density of 2.47 $g.cm^{-3}$ was obtained at 1650 °C with the HD powder, as

noted in **Table 2**. The difficulty to obtain fully dense materials from the TK powder was related to the higher amount of boric acid and its premature volatilization during heating This phenomenon could induce the formation of closed porosity (by the development of gas occlusion), which are difficult to eliminate. The determined densities values allow estimations of relative densities to 96.2 and 99.0 % respectively. Although the chemical compositions of the materials are different, both XRD diffractograms from sintered samples were found to correspond to JCPDS 01-075-0424 card with a radiocrystallographic density of 2.495 $g.cm^{-3}$. As a consequence, this latter was chosen as reference for boron oxycarbide instead of the commonly admitted value for boron carbide of 2.52 $g.cm^{-3}$.

A typical SEM micrograph of the 99 %TD HD sample sintered at 1650°C is displayed in **Figure 6.a.** Some graphite layers can be observed in a few pores exhibiting an "onion-like" shape, as represented in **Figure 6.b.** (white arrow) **or Figure 4.e,** and as already observed by Belon *et al.* [21]. **Table 3** references grain sizes in the range 100 to 2000 nm, with a mean diameter of 564 nm. Besides, the microstructure of TK sample sintered at 1550 °C (relative density of 96.2 %) exhibits smaller grains ranged from 10 to 400 nm, as seen in **Figure 6**.**c**, with a mean diameter of approximately 82 nm. Consequently, both powders exhibit limited grain growth for these sintering conditions.

3.1. Mechanical properties

Mechanical properties (i.e. elasticity and hardness) of sintered samples, which are determined at the macroscopic and microscopic scales, are displayed in **Table 3**.

The fully dense HD material exhibits a Knoop hardness of 22.8 ± 2 GPa and an apparent Young Modulus of 448 ± 3 GPa. This last value is close to the properties measured by ultrasonic means reported for fully dense boron carbides [15,17]. Moreover, apparent hardness was also measured using a Vickers indenter to compare sintered materials with the literature data. In fact, this technique is commonly used in research papers but in this case, due to damage under Vickers indentations, the Knoop indenter was preferred to limit experimental errors. The HD monolith exhibits a Vickers hardness of 31.8 ± 1.4 GPa, which is in good agreement with the literature [15,38].

The mechanical properties characterization was carried out sintered materials exhibiting exactly the same relative densities (*i.e*. 92 and 96 %). At the macroscopic scale, for a relative density of 96 %, the HD sample presents a Knoop hardness of 18.6 GPa, which is higher than the TK one which was found to be 16.9 GPa. In addition, the HD sample is more rigid with an apparent Young's modulus of 395 GPa while only 370 GPa was found for TK. These Young's modulus values are in the range of those measured by Sairam *et al.* [17] and Hayun *et al.* [15] in 96 %TD boron carbides. The same tendency for both materials has been observed at a lower relative density of 92 %. The elasticity and the hardness were inferior by 11-14 % for TK samples. Consequently, in spite of the TK significantly lower grain size, HD samples show improved mechanical properties. This observation could be extended to the different relative density levels.

At the microscopic scale, the nanoindentation experiments reveal the bulk mechanical properties of both materials, with a limited effect of the grain boundaries.

Indeed, the mechanical response is characterized within the depth range 200-300 nm, which is lower than the grain size of the HD sample and in the same order for the TK sample. As usual, for both materials, the intrinsic elasticity and hardness are higher than the relative apparent properties. The TK material exhibits intrinsic hardness and Young's modulus slightly lower by about 20 % compared to the HD sample.

3.2. Discussion

Although TK sintered specimen exhibits a finer grain size, its mechanical properties are lower compared to the HD material. This result is surprising as it disagrees with the Hall-Petch law commonly observed for ceramics, according to which the lower the grain size the higher the mechanical properties (especially hardness).. This dissimilarity in intrinsic properties could hence be related to their different chemical composition. Indeed, the influence of the chemical composition of the material has to be considered as a key parameter in the mechanical response in carbide materials. This difference in chemical composition directly affects their mechanical properties. Indeed, as previously shown by Niihara *et al.* [39], a difference in the B/C ratio can affect the hardness. The measured B/C ratios of HD and TK materials are reported on this abacus, displayed in **Figure 7.a**, as well as a reference material MT [22]. The hardness of HD and MT samples seems to be in accordance with the evolution of hardness with the B/C ratio. However, the hardness value of the TK material is apart from the values measured by Niihara *et al.* [39] for an equivalent B/C ratio. Therefore, the higher oxygen content of TK materials seems to be the main parameter explaining this difference in mechanical behaviour. During sintering, the boric acid is almost totally removed. However, the remaining oxygen in the monoliths is involved in boron oxycarbide ceramics, $B_{3.83}CO_{0.04}$ and $B_{4.59}CO_{0.18}$ for HD and TK respectively. The position

of the oxygen atom within the boron oxycarbide is unknown from the literature as it could fill a vacancy or, as for Ti-C-O or Zr-C-O, substitutes the carbon [40,41].

The lower apparent hardness and elasticity of TK material is a consequence of the lower intrinsic properties of the oxycarbide phase. This phenomenon has already been reported by Réjasse *et al.* [22] where a decrease of the Young modulus was found when increasing the oxygen amount in fully dense boron carbide specimens having similar grain sizes. Moreover, as depicted in **Figure 7.b**, it was also observed a decrease in the intrinsic hardness, which is in agreement with the values of this work**.** So, the higher oxygen content of the TK sample also induces a lower rigidity.

Indeed, it is shown that the stoichiometry has a deeper impact than grain size for a similar relative density. Therefore, this work highlights the necessity to control the stoichiometry in order to elaborate boron oxycarbide compounds with improved mechanical properties. To maximize sample hardness, it is necessary to optimize the B/C ratio around 4 and to lower the structural oxygen content within the oxycarbide phase, which have been proved to be detrimental for the mechanical behavior.

4. Conclusion

This study clearly highlights the importance of the measurement of oxygen content on the mechanical properties on carbides. Two boron carbide powders with different mean grain sizes, one submicronic (HD) and one nanometric (TK), were sintered by SPS. The chemical analyzes reveal that sintered samples are in reality boron oxycarbide ceramics, *i.e.* $B_{3.83}CO_{0.04}$ and $B_{4.59}CO_{0.18}$ for HD and TK monoliths respectively. The mechanical properties of SPS sintered specimens were compared at similar relative densities of 92 and 96 % with a significant difference in mean grain size, *i.e.* 90 and

400 nm for the TK and HD materials respectively. Even if the TK monolith exhibits finer grain size, it was found that the apparent hardness and elasticity were higher for the HD materials. This shift in the Hall-Petch law and more generally in the mechanical properties is explained by the leading effect of structural oxygen content in the boron oxycarbide ceramics. Consequently, to enhance mechanical behavior of boron carbides from the submicronic to the nanometric scale, it is shown the importance to already monitor the stoichiometry at the powder synthesis step as these materials tends easily to form weaker boron oxycarbide phases.

Acknowledgements

The authors gratefully thank Marion Vandenhende from IRCER Institute for her help in carrying out SPS experiments and Dr Gaëlle Gutierrez from CEA Saclay for Raman spectroscopy experiments at the JANNUS-Saclay facility.

References

[1] F. Thevenot, Boron carbide - a comprehensive review, J. Eur. Ceram. Soc. 6 (1990) 205–225. doi:https://doi.org/10.1016/0955-2219(90)90048-K.

[2] A.K. Suri, C. Subramanian, J.K. Sonber, T.S.R.C. Murthy, Synthesis and consolidation of boron carbide: a review, Int. Mater. Rev. 55 (2010) 4–40. doi:10.1179/095066009X12506721665211.

[3] D. Gosset, P. Herter, Matériaux absorbants neutroniques pour le pilotage des réacteurs, Tech. Ing. Génie Nucl. (2007).

[4] L. Vargas-Gonzalez, R.F. Speyer, J. Campbell, Flexural Strength, Fracture Toughness, and Hardness of Silicon Carbide and Boron Carbide Armor Ceramics, Int. J. Appl. Ceram. Technol. 7 (2010) 643–651. doi:10.1111/j.1744-7402.2010.02501.x.

[5] B.M. Moshtaghioun, D. Gomez-Garcia, A. Dominguez-Rodriguez, R.I. Todd, Abrasive wear rate of boron carbide ceramics: Influence of microstructural and mechanical aspects on their tribological response, J. Eur. Ceram. Soc. 36 (2016) 3925–3928. doi:10.1016/j.jeurceramsoc.2016.06.029.

[6] T.R. Chapman, D.E. Niesz, R.T. Fox, T. Fawcett, Wear-resistant aluminum–boron–carbide cermets for automotive brake applications, Wear. 236 (1999) 81–87. doi:10.1016/S0043-1648(99)00259-8.

[7] A. Gerbershagen, C. Baumgarten, D. Kiselev, R. van der Meer, Y. Risters, Marco Schippers, Measurements and simulations of boron carbide as degrader material for proton therapy, Phys. Med. Biol. 61 (2016) N337. doi:10.1088/0031-9155/61/14/N337.

[8] R.W. Rice, C.C. Wu, F. Boichelt, Hardness–Grain-Size Relations in Ceramics, J. Am. Ceram. Soc. 77 (1994) 2539–2553. doi:10.1111/j.1151-2916.1994.tb04641.x.

[9] A. Krell, P. Blank, Grain Size Dependence of Hardness in Dense Submicrometer Alumina, J. Am. Ceram. Soc. 78 (1995) 1118–1120. doi:10.1111/j.1151-2916.1995.tb08452.x.

[10] A. Krell, A. Bales, Grain Size-Dependent Hardness of Transparent Magnesium Aluminate Spinel, Int. J. Appl. Ceram. Technol. 8 (2011) 1108–1114. doi:10.1111/j.1744-7402.2010.02583.x.

[11] J.A. Wollmershauser, B.N. Feigelson, E.P. Gorzkowski, C.T. Ellis, R. Goswami, S.B. Qadri, J.G. Tischler, F.J. Kub, R.K. Everett, An extended hardness limit in bulk nanoceramics, Acta Mater. 69 (2014) 9–16. doi:10.1016/j.actamat.2014.01.030.

[12] H. Lee, R.F. Speyer, Pressureless Sintering of Boron Carbide, J. Am. Ceram. Soc. 86 (2003) 1468–1473. doi:https://doi.org/10.1111/j.1151-2916.2003.tb03498.x.

[13] S.L. Dole, S. Prochazka, R.H. Doremus, Microstructural Coarsening During Sintering of Boron Carbide, J. Am. Ceram. Soc. 72 (1989) 958–966. doi:https://doi.org/10.1111/j.1151-2916.1989.tb06252.x.

[14] R. Angers, M. Beauvy, Hot-pressing of boron carbide, Ceram. Int. 10 (1984) 49–55. doi:https://doi.org/10.1016/0272-8842(84)90025-7.

[15] S. Hayun, V. Paris, M.P. Dariel, N. Frage, E. Zaretzky, Static and dynamic mechanical properties of boron carbide processed by spark plasma sintering, J. Eur. Ceram. Soc. 29 (2009) 3395–3400. doi:10.1016/j.jeurceramsoc.2009.07.007.

[16] S. Hayun, S. Kalabukhov, V. Ezersky, M.P. Dariel, N. Frage, Microstructural characterization of spark plasma sintered boron carbide ceramics, Ceram. Int. 36 (2010) 451–457. doi:10.1016/j.ceramint.2009.09.004.

[17] K. Sairam, J.K. Sonber, T.S.R.C. Murthy, C. Subramanian, R.K. Fotedar, P. Nanekar, R.C. Hubli, Influence of spark plasma sintering parameters on densification and mechanical properties of boron carbide, Int. J. Refract. Met. Hard Mater. 42 (2014) 185–192. doi:10.1016/j.ijrmhm.2013.09.004.

[18] X. Li, D. Jiang, J. Zhang, Q. Lin, Z. Chen, Z. Huang, Densification behavior and related phenomena of spark plasma sintered boron carbide, Ceram. Int. 40 (2014) 4359–4366. doi:10.1016/j.ceramint.2013.08.106.
[19] B.M. Moshtaghioun, F.L. Cumbrera, A.L. Ortiz, M. Castillo-Rodríguez, D. Gómez-García, Additive-free superhard B4C with ultrafine-grained dense microstructures, J. Eur. Ceram. Soc. 34 (2014) 841–848. doi:10.1016/j.jeurceramsoc.2013.10.006.
[20] B.M. Moshtaghioun, D. Gómez-García, A. Domínguez-Rodríguez, A.L. Ortiz, Enhancing the spark-plasma sinterability of B4C nanopowders via room-temperature methylation induced purification, J. Eur. Ceram. Soc. 36 (2016) 2843–2848. doi:10.1016/j.jeurceramsoc.2016.04.008.
[21] R. Belon, G. Antou, N. Pradeilles, A. Maître, D. Gosset, Mechanical behaviour at high temperature of spark plasma sintered boron carbide ceramics, Ceram. Int. 43 (2017) 6631–6635. doi:10.1016/j.ceramint.2017.02.053.
[22] F. Réjasse, M. Georges, N. Pradeilles, G. Antou, A. Maître, Influence of chemical composition on mechanical properties of spark plasma sintered boron carbide monoliths, J. Am. Ceram. Soc. 101 (2018) 3767–3772. doi:10.1111/jace.15707.
[23] B.M. Moshtaghioun, D. Gomez-Garcia, A. Dominguez-Rodriguez, R.I. Todd, Grain size dependence of hardness and fracture toughness in pure near fully-dense boron carbide ceramics, J. Eur. Ceram. Soc. 36 (2016) 1829–1834. doi:10.1016/j.jeurceramsoc.2016.01.017.
[24] W.C. Oliver, G.M. Pharr, An improved technique for determining hardness and elastic modulus using load and displacement sensing indentation experiments, J. Mater. Res. 7 (1992) 1564–1583.
[25] A. Jay, Conception in silico d'une nouvelle phase de carbure de bore, Thèse de l'École Polytechnique, Université Paris-Saclay., 2015.
[26] G. Victor, Etude des modifications structurales induites dans le carbure de bore B4C par irradiation aux ions dans différents domaines d'énergie, Thèse de l'Université de Lyon, 2016.
[27] J. Huguet-Garcia, A. Jankowiak, S. Miro, D. Gosset, Y. Serruys, J.-M. Costantini, Study of the Ion-Irradiation Behavior of Advanced SiC Fibers by Raman Spectroscopy and Transmission Electron Microscopy, J. Am. Ceram. Soc. 98 (2015) 675–682. doi:10.1111/jace.13342.
[28] D. Gosset, S. Miro, S. Doriot, G. Victor, V. Motte, Evidence of amorphisation of boron carbide under slow, heavy ion irradiation, Nucl. Instrum. Methods Phys. Res. Sect. B Beam Interact. Mater. At. 365 (2015) 300–304. doi:10.1016/j.nimb.2015.07.054.
[29] F. Tuinstra, J.L. Koenig, Raman Spectrum of Graphite, J. Chem. Phys. 53 (1970) 1126–1130. doi:10.1063/1.1674108.
[30] M.A. Rossi, M.J. Matthewson, A. Kaza, D. Niesz, R.L. Haber, Modeling of Gas-Phase Transport and Composition Evolution during the Initial-Stage Sintering of Boron Carbide with Carbon Additions, J. Am. Ceram. Soc. 93 (2010) 3691–3699. doi:10.1111/j.1551-2916.2010.03973.x.
[31] B.M. Moshtaghioun, A.L. Ortiz, D. Gómez-García, A. Domínguez-Rodríguez, Densification of B4C nanopowder with nanograin retention by spark-plasma sintering, J. Eur. Ceram. Soc. 35 (2015) 1991–1998. doi:10.1016/j.jeurceramsoc.2014.12.021.
[32] M. Asadikiya, C. Rudolf, C. Zhang, B. Boesl, A. Agarwal, Y. Zhong, Thermodynamic modeling and investigation of the oxygen effect on the sintering of B4C, J. Alloys Compd. 699 (2017) 1022–1029. doi:10.1016/j.jallcom.2016.12.315.
[33] D.R. Tallant, T.L. Aselage, A.N. Campbell, D. Emin, Boron carbide structure by Raman spectroscopy, Phys. Rev. B. 40 (1989) 5649–5656. doi:10.1103/PhysRevB.40.5649.
[34] C. Cheng, K.M. Reddy, A. Hirata, T. Fujita, M. Chen, Structure and mechanical properties of boron-rich boron carbides, J. Eur. Ceram. Soc. 37 (2017) 4514–4523. doi:10.1016/j.jeurceramsoc.2017.06.017.

[35] K.Y. Xie, V. Domnich, L. Farbaniec, B. Chen, K. Kuwelkar, L. Ma, J.W. McCauley, R.A. Haber, K.T. Ramesh, M. Chen, K.J. Hemker, Microstructural characterization of boron-rich boron carbide, Acta Mater. 136 (2017) 202–214. doi:10.1016/j.actamat.2017.06.063.
[36] A. Jay, N. Vast, J. Sjakste, O.H. Duparc, Carbon-rich icosahedral boron carbide designed from first principles, Appl. Phys. Lett. 105 (2014) 031914. doi:10.1063/1.4890841.
[37] B.M. Moshtaghioun, D. Gómez-García, A.D. Rodríguez, Exotic grain growth law in twinned boron carbide under electric fields, J. Eur. Ceram. Soc. 38 (2018) 4590–4596. doi:10.1016/j.jeurceramsoc.2018.06.029.
[38] B.M. Moshtaghioun, F.L. Cumbrera-Hernández, D. Gómez-García, S. de Bernardi-Martín, A. Domínguez-Rodríguez, A. Monshi, M.H. Abbasi, Effect of spark plasma sintering parameters on microstructure and room-temperature hardness and toughness of fine-grained boron carbide (B4C), J. Eur. Ceram. Soc. 33 (2013) 361–369. doi:10.1016/j.jeurceramsoc.2012.08.028.
[39] K. Niihara, A. Nakahira, T. Hirai, The Effect of Stoichiometry on Mechanical Properties of Boron Carbide, J. Am. Ceram. Soc. 67 (2006) C-13-C–14. doi:10.1111/j.1151-2916.1984.tb19158.x.
[40] F. Réjasse, O. Rapaud, G. Trolliard, O. Masson, A. Maître, Experimental investigation and thermodynamic evaluation of the C–O–Zr ternary system, RSC Adv. 6 (2016) 100122–100135. doi:10.1039/C6RA21967E.
[41] F. Réjasse, O. Rapaud, J. Léchelle, G. Trolliard, H. Khodja, O. Masson, G. Martin, A. Maître, Novel insight into the chemical analysis of light elements in oxycarbides, Acta Mater. 157 (2018) 11–20. doi:10.1016/j.actamat.2018.07.023.
[42] V. Domnich, S. Reynaud, R.A. Haber, M. Chhowalla, Boron Carbide: Structure, Properties, and Stability under Stress, J. Am. Ceram. Soc. 94 (2011) 3605–3628. doi:10.1111/j.1551-2916.2011.04865.x.
[43] N. Cho, K.G. Silver, Y. Berta, R.F. Speyer, N. Vanier, C.-H. Hung, Densification of carbon-rich boron carbide nanopowder compacts, J. Mater. Res. 22 (2007) 1354–1359. doi:10.1557/jmr.2007.0155.

Figure captions

Figure 1: XRD patterns of as-received powders and sintered samples. COLOUR SHOULD BE USED

Figure 2 : Raman spectra of as-received powders and sintered samples. Peak identification reported by [25]. COLOUR SHOULD BE USED

Figure 3 : Particle size distribution (in number) for HD and TK powders at 1650 °C (HD) and at 1550 °C (TK). COLOUR SHOULD BE USED

Figure 4 : SEM images (a, b) and TEM observations (c, d, e, f) of HD and TK powders. COLOUR SHOULD BE USED

Figure 5 : Normalized shrinkage rates measured during the SPS treatment of boron carbide powders. COLOUR SHOULD BE USED

Figure 6 : SEM micrographs of a,b) HD sample sintered at 1650 °C and c) TK sample sintered at 1550 °C (after thermal etching). Note: exaggerated grain growth is observed in b) due to the post heat treatment applied to reveal grain boundaries.

Figure 7 : Evolution of hardness with a) the B/C content and b) the oxygen content. COLOUR SHOULD BE USED

Tables

***Table 1**: Elemental chemical analyses carried out on powders and sintered samples.*

		wt% O	wt% H	wt% C	wt% B *
HD	Powder	**2.51** ± 0.07	**0.19** ± 0.01	**22.8** ± 0.4	**≃ 74**
	Bulk	**1.31** ± 0.18	**0.01** ± 0.01	**22.2** ± 0.3	**≃ 76**
TK	Powder	**6.02** ± 0.16	**0.35** ± 0.01	**17.6** ± 1.0	**≃ 76**
	Bulk	**4.50** ± 0.15	**0.03** ± 0.01	**18.6** ± 0.2	**≃ 77**

* Obtained by subtraction

***Table 2**: Open porosity and density of sintered samples. The theoretical density used to determine the relative density was the radiocrystallographic density (2.495 g.cm^{-3}).*

	Sintering temperature (°C)	Open porosity (%)	Density (g.cm^{-3})	Relative density (%)
HD	1700	< 1	2.47	99.0
	1650	< 1	2.47	99.0
	1525	< 1	2.45	98.0
	1475	1.9	2.41	96.4
	1450	6.0	2.29	91.9
	1425	15.6	2.11	84.7
	1400	28.8	1.78	71.4
TK	1550	1.1	2.40	96.2
	1400	2.1	2.29	91.9
	1350	9.6	2.10	84.2

***Table 3**: Microstructure features and mechanical properties of sintered samples.*

	HD	**HD**	**HD**	**TK**	**TK**
Relative density (%)	> 99	96.4	91.9	96.2	91.9
Grain size (nm)					
Mean diameter	564 ± 270	474 ± 220	444 ± 160	82 ± 50	74 ± 60
Range	105 - 1940	150 - 1570	70 – 1270	10 - 400	15 - 260
At the grain scale					
Nano-hardness (GPa)		45 ± 2		35 ± 2	
Intrinsic Young Modulus (GPa)		465 ± 23		380 ± 26	
At the macroscopic scale					
Knoop hardness (GPa)	22.8 ± 2	18.6 ± 1	15.0 ± 1	16.9 ± 1	13.9 ± 1
Apparent Young modulus (GPa)	448 ± 3	395 ± 12	370 ± 10	369 ± 10	317 ± 10
Apparent shear modulus (GPa)	189 ± 2	167 ± 5	155 ± 4	152 ± 5	132 ± 4

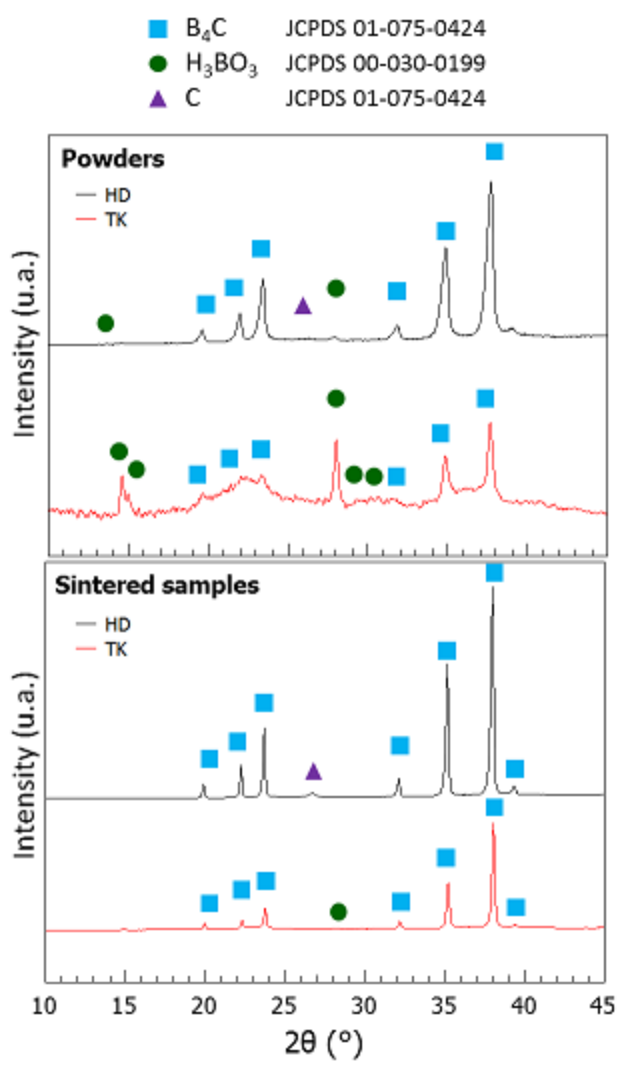
B4C JCPDS 01-075-0424
H3BO3 JCPDS 00-030-0199
C JCPDS 01-075-0424
Powders
HD
TK
Intensity (u.a.)
Sintered samples
HD
TK
Intensity (u.a.)
10
15
20
25
30
35
40
45
2θ (°)

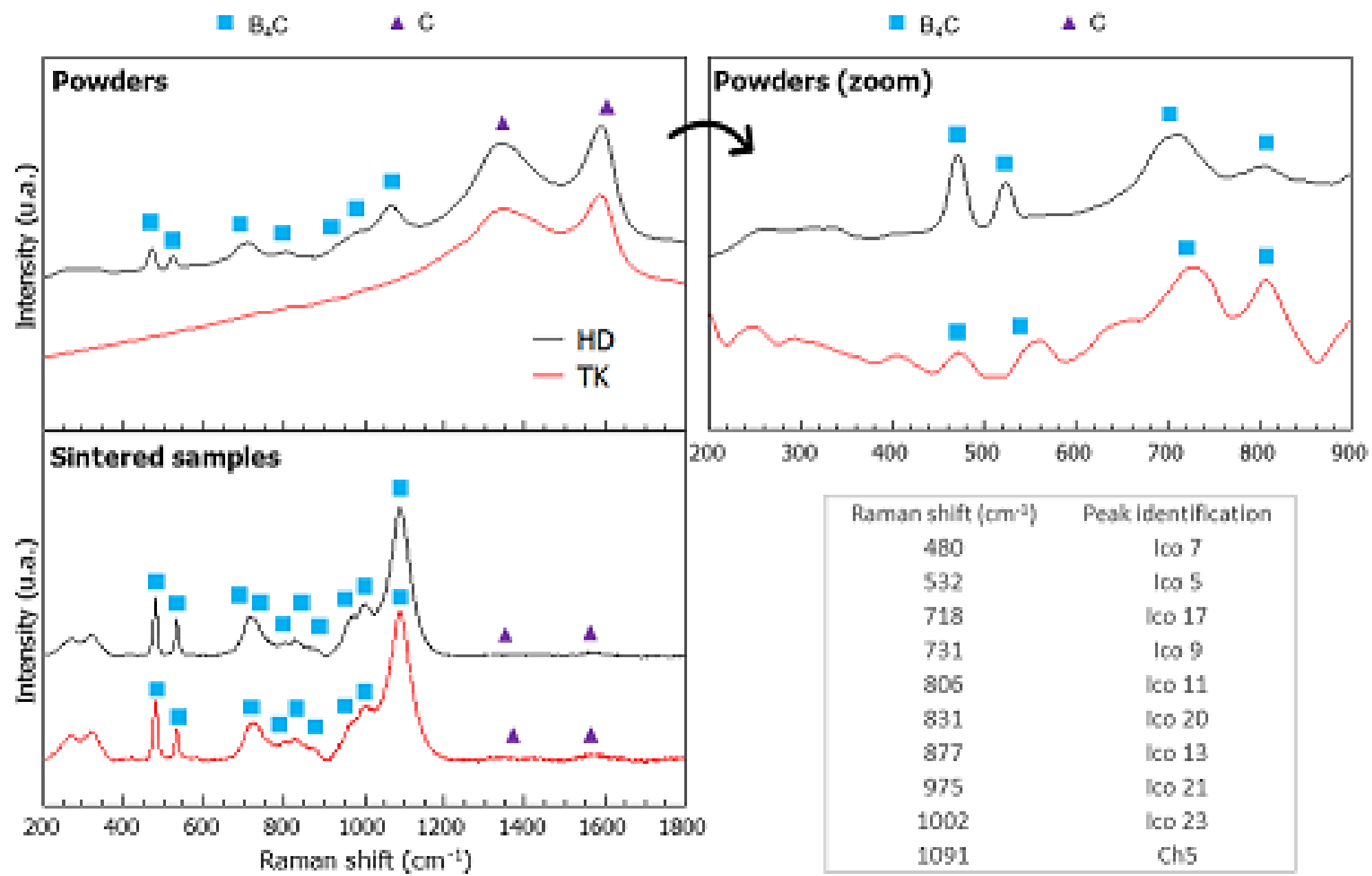

Raman shift (cm^{-1})	Peak identification
480	Ico 7
532	Ico 5
718	Ico 17
731	Ico 9
806	Ico 11
831	Ico 20
877	Ico 13
975	Ico 21
1002	Ico 23
1091	Ch5

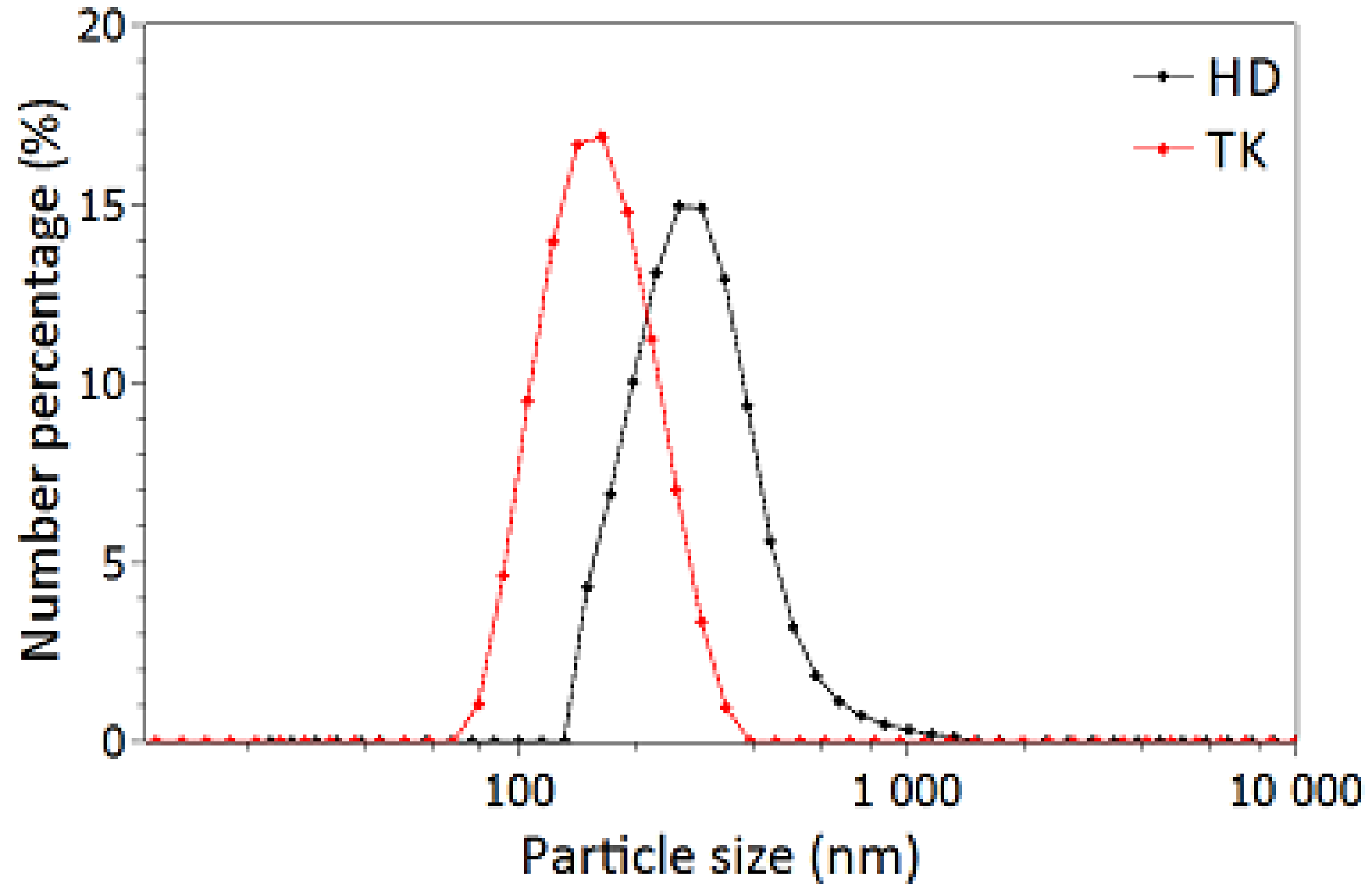
20
15
10
5
0
Number percentage (%)
HD
TK
100
1 000
10 000
Particle size (nm)

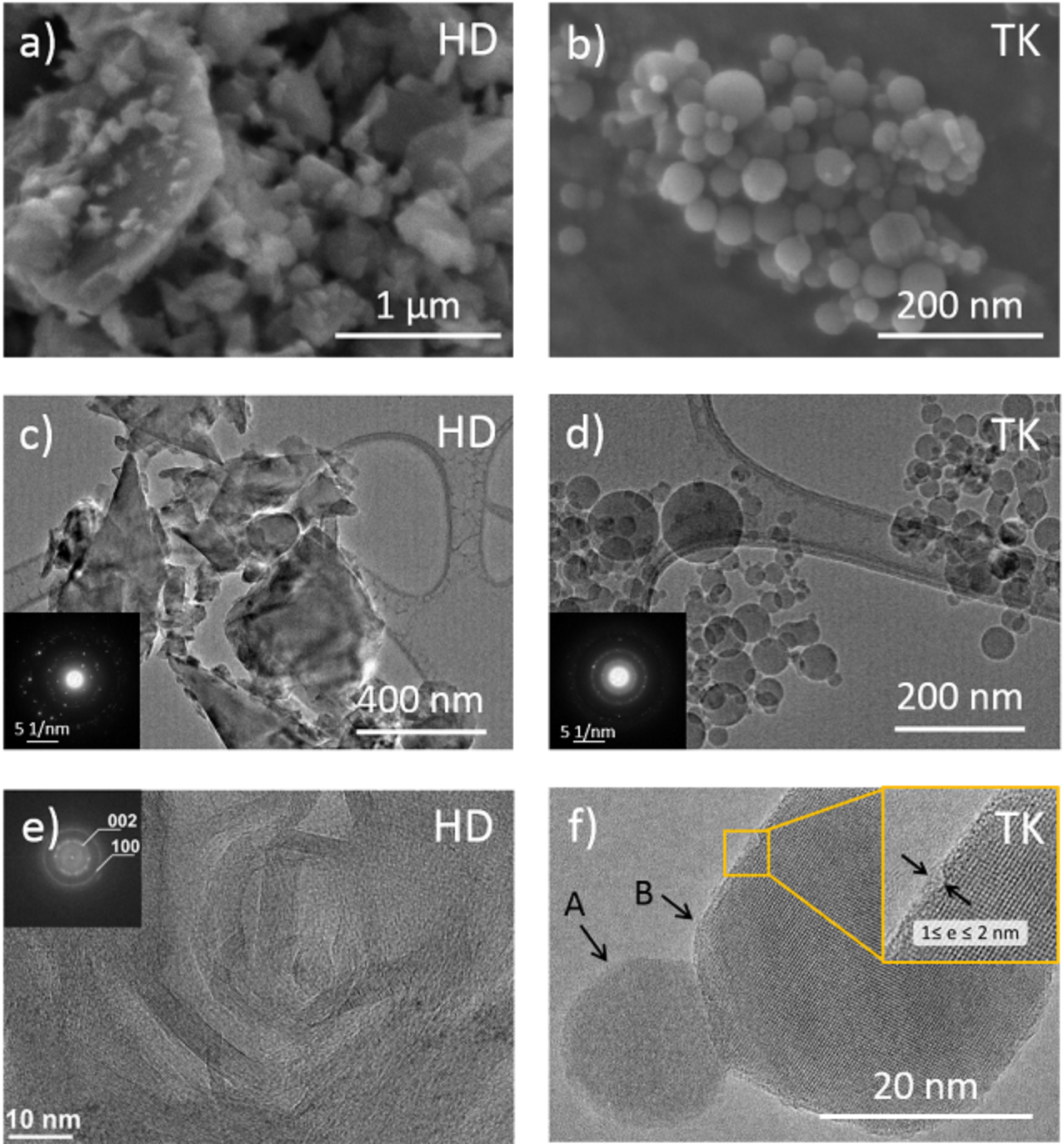
a)
HD
1 µm
b)
TK
200 nm
c)
HD
5 1/nm
400 nm
d)
TK
5 1/nm
200 nm
e)
002
100
HD
10 nm
f)
A
B
TK
1≤ e ≤ 2 nm
20 nm

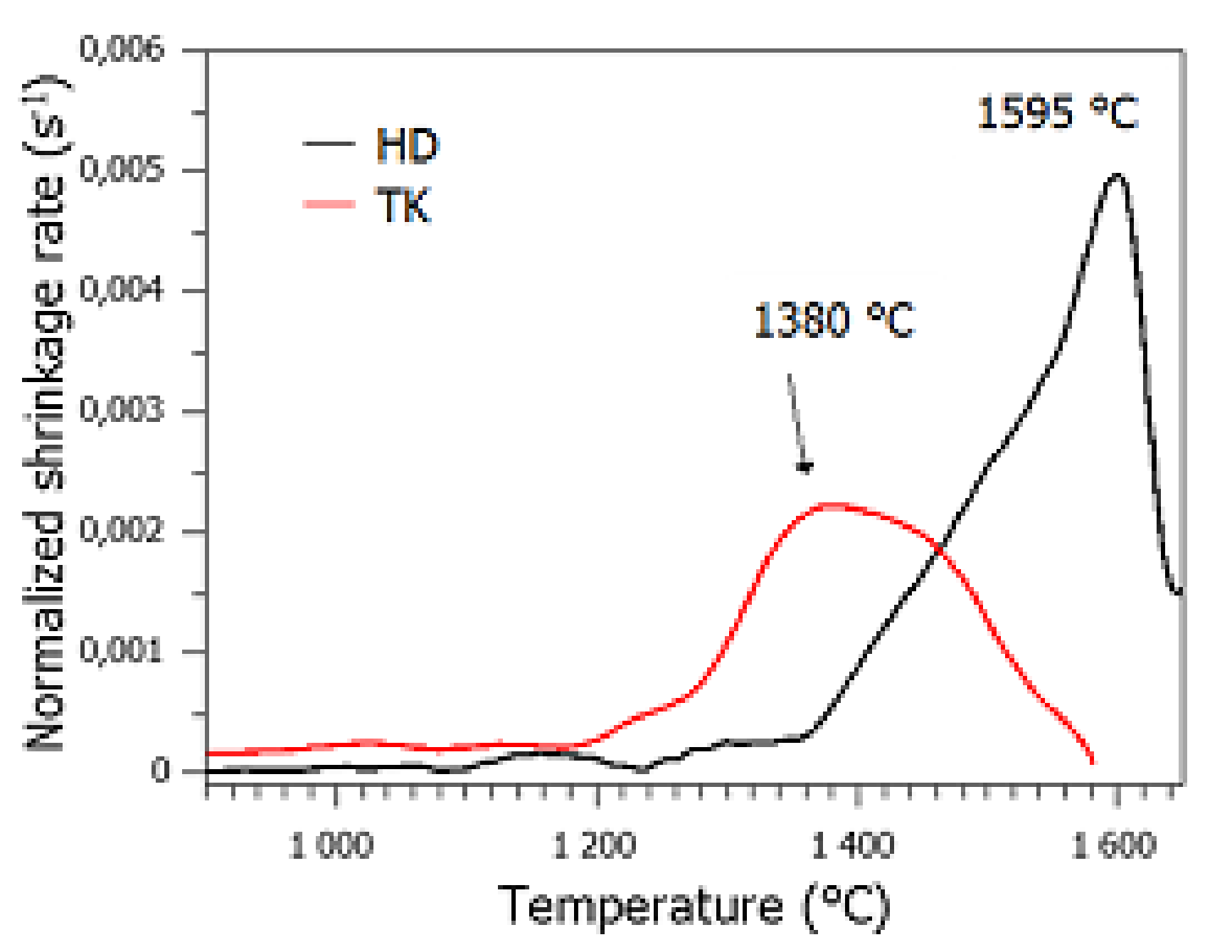
0,006
0,005
0,004
0,003
0,002
0,001
0
Normalized shrinkage rate (s-1)
HD
TK
1595 °C
1380 °C
1 000
1 200
1 400
1 600
Temperature (°C)

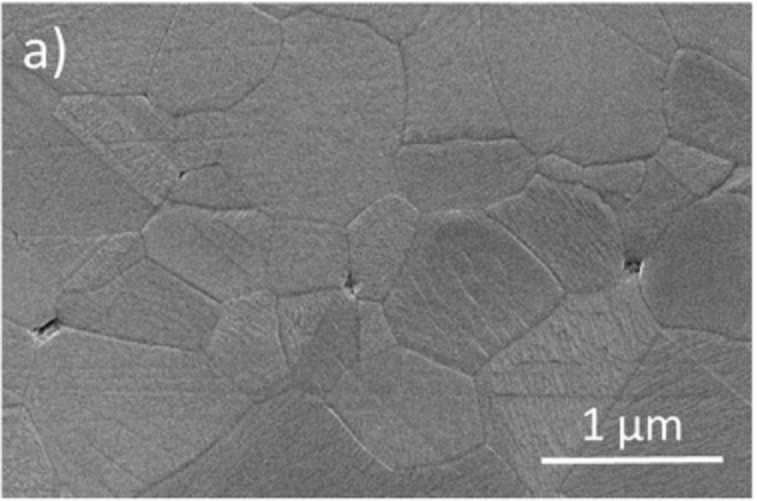
a)
1 µm

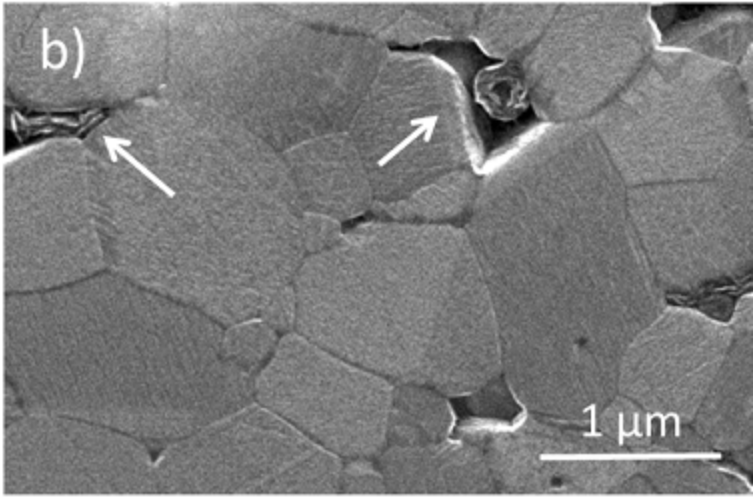
b)
1 µm

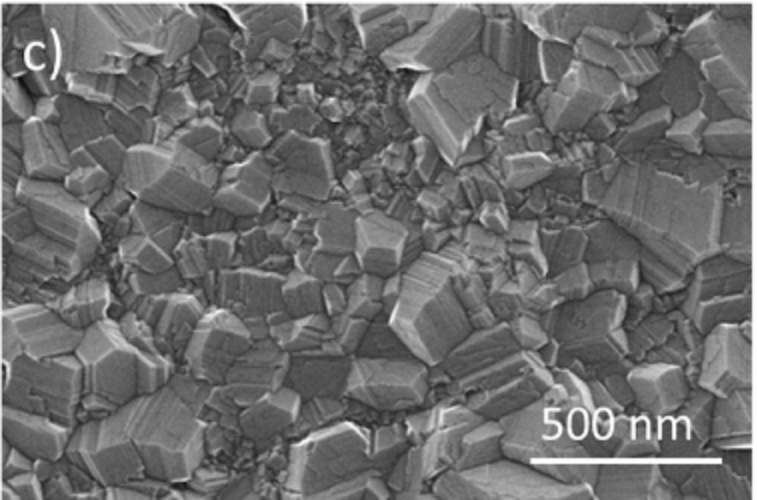
c)
500 nm

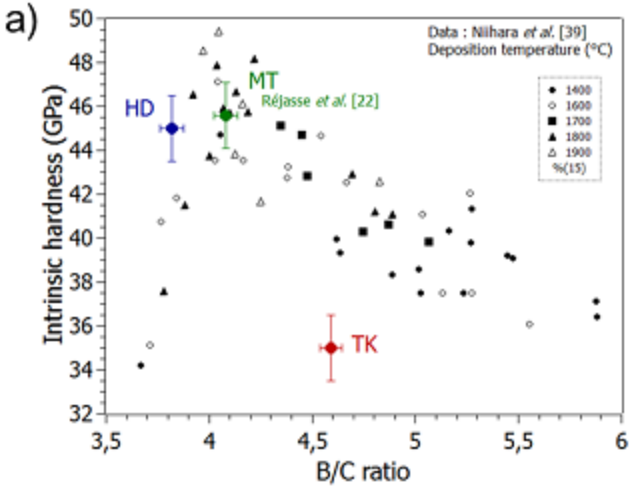
a)
Data : Nihara et al. [39]
Deposition temperature (°C)
1400
1600
1700
1800
1900
%(15)
MT
Réjasse et al. [22]
HD
TK
Intrinsic hardness (GPa)
B/C ratio
50
48
46
44
42
40
38
36
34
32
3,5
4
4,5
5
5,5
6

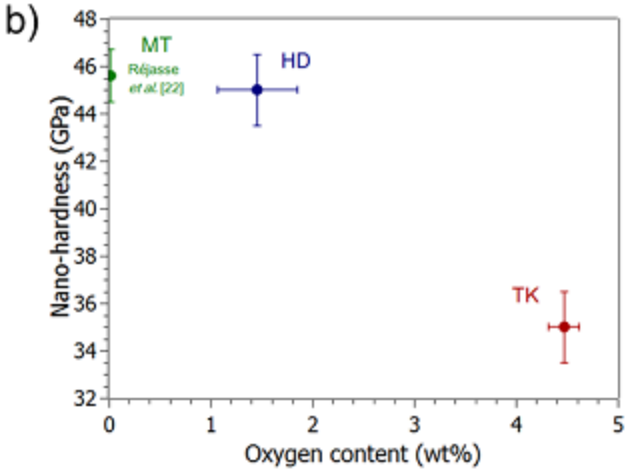
b)
MT
Réjasse
et al. [22]
HD
TK
Nano-hardness (GPa)
Oxygen content (wt%)
48
46
44
42
40
38
36
34
32
0
1
2
3
4
5